Supplementary Information (SI) for Nanoscale.
This journal is © The Royal Society of Chemistry 2026

Engineering Osteoinductive Hydroxyapatite via Zinc and Strontium Co-Substitution

Sivaraj Durairaj[1]*, Malika Arora[2], Satish Kumar[2], Preethi Murugesan[2], Juan F. Vivanco[1], Deepa Ghosh[2]*

[1]*Faculty of Engineering and Sciences, Universidad Adolfo Ibáñez, Viña del Mar, 2580335, Chile.*

[2]*Chemical Biology Unit, Institute of Nanoscience and Technology, Knowledge City, Sector 81, Mohali 140306, Punjab, India*

*Corresponding authors: siva191091@gmail.com (Sivaraj Durairaj); deepa.ghosh@inst.ac.in (Deepa Ghosh)

Supporting Information

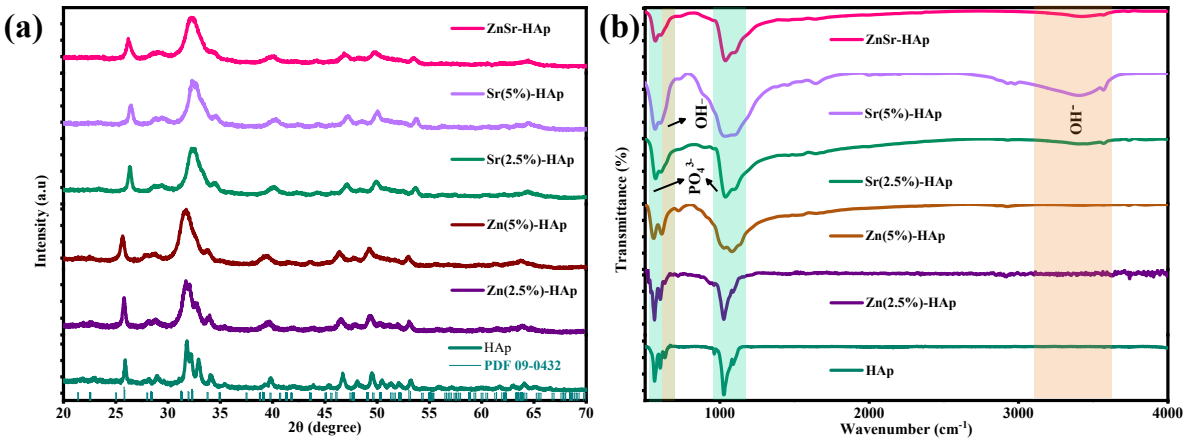

Figure S1. (a) X-ray diffraction patterns of pristine, Zn, Sr, and ZnSr incorporated HAp nanoparticles. (b) Fourier transform infrared spectroscopy spectra of pristine, Zn, Sr, and ZnSr incorporated HAp nanoparticles.

Table S1 Lattice parameters, average crystallite size, and dislocation density

Sample	Lattice Parameter (Å)		Unit Cell Volume $(Å)^3$	Micro strain	Average Crystallite Size (nm)	Dislocation density
	a	C				
Pristine HAp	0.9409	0.6876	527.14	0.2590	24.64	0.000856

2.5Zn	0.9438	0.69025	530.72	0.3104	18.86	0.001222
5Zn	0.9449	0.6944	535.25	0.3521	16.68	0.001569
2.5Sr	0.9262	0.676	511.93	0.3918	15.65	0.002022
5Sr	0.9238	0.6738	508.43	0.4656	13.80	0.002869
ZnSr	0.9318	0.6788	517.07	0.6048	11.59	0.004759

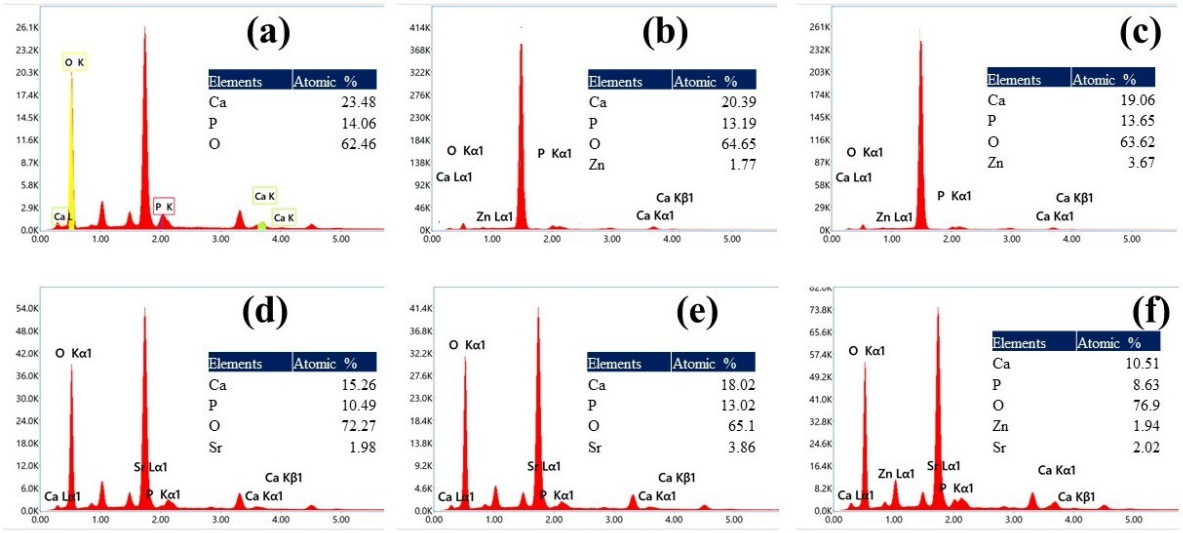

Figure S2. Energy dispersive X-ray spectra of (a) HAp; (b) Zn (2.5%)-HAp, (c) Zn (5%)-HAp, (d) Sr (2.5%)-HAp, (e) Sr (5%)-HAp, and (f) ZnSr incorporated HAp nanoparticles.

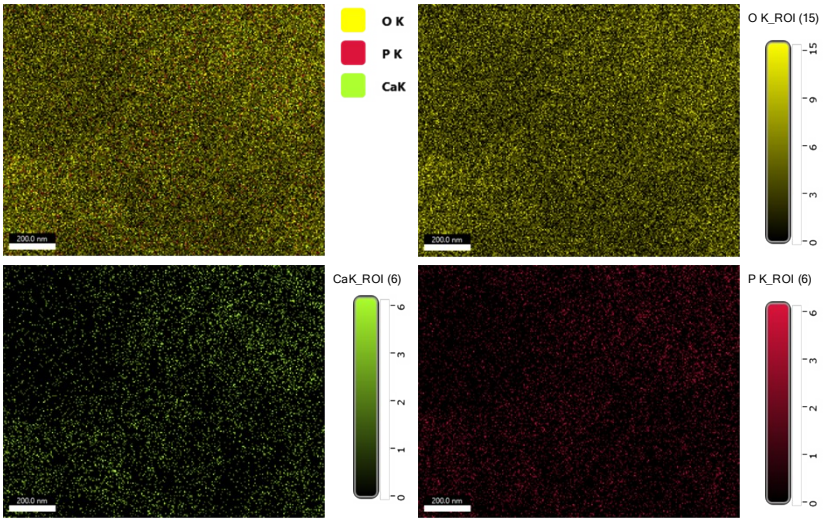

Figure S3. EDX mapping of HAp nanoparticles.

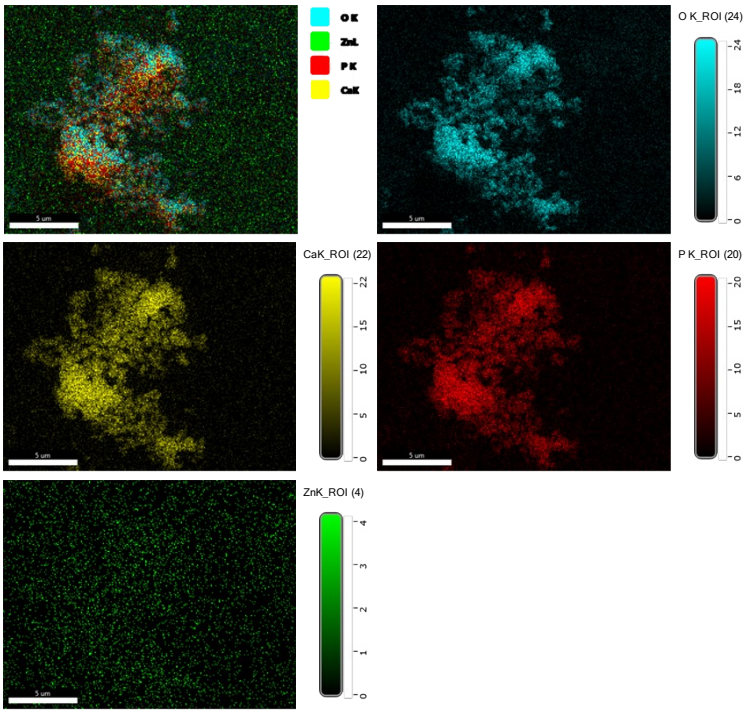

Figure S4. EDX mapping of Zn (2.5%)-HAp nanoparticles.

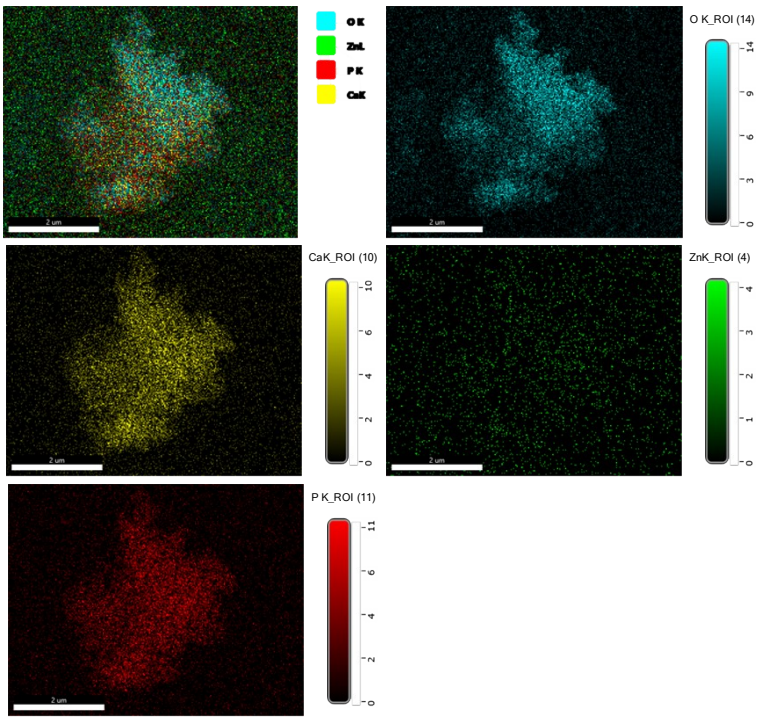

Figure S5. EDX mapping of Zn (5%)-HAp nanoparticles

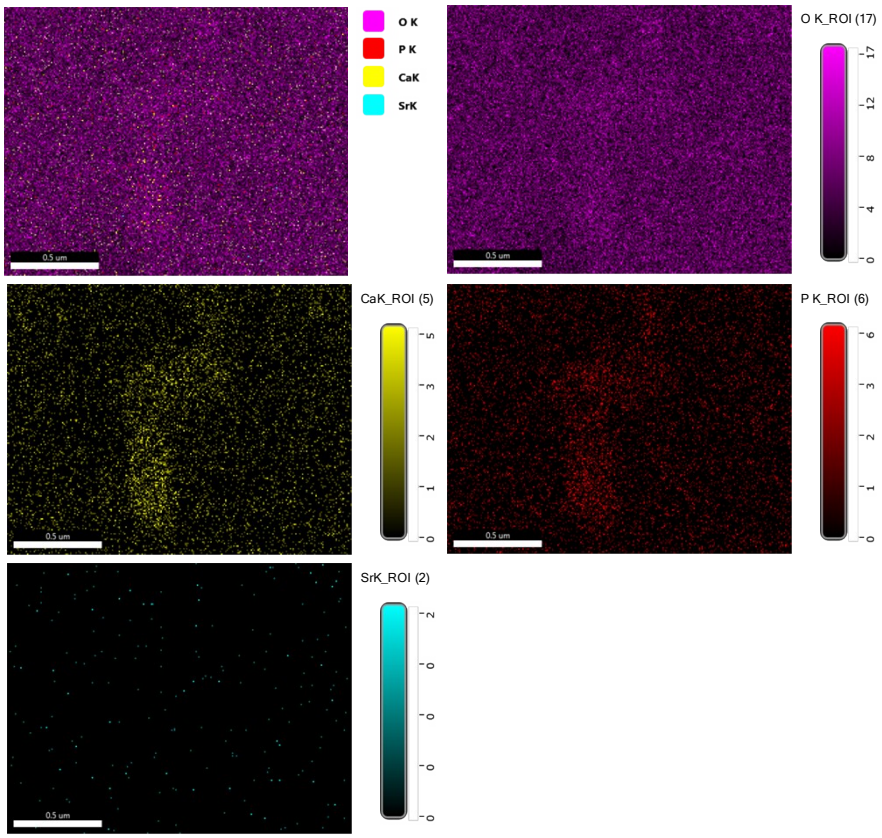

Figure S6. EDX mapping of Sr (2.5%)-HAp nanoparticles.

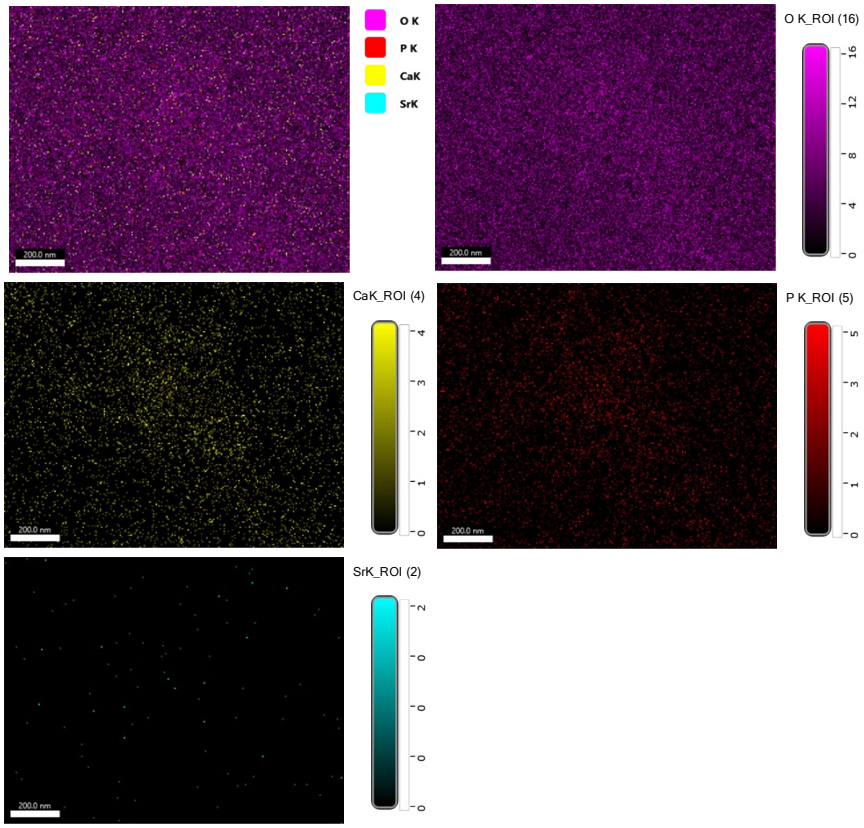

Figure S7. EDX mapping of Sr(5%)-HAp nanoparticles.

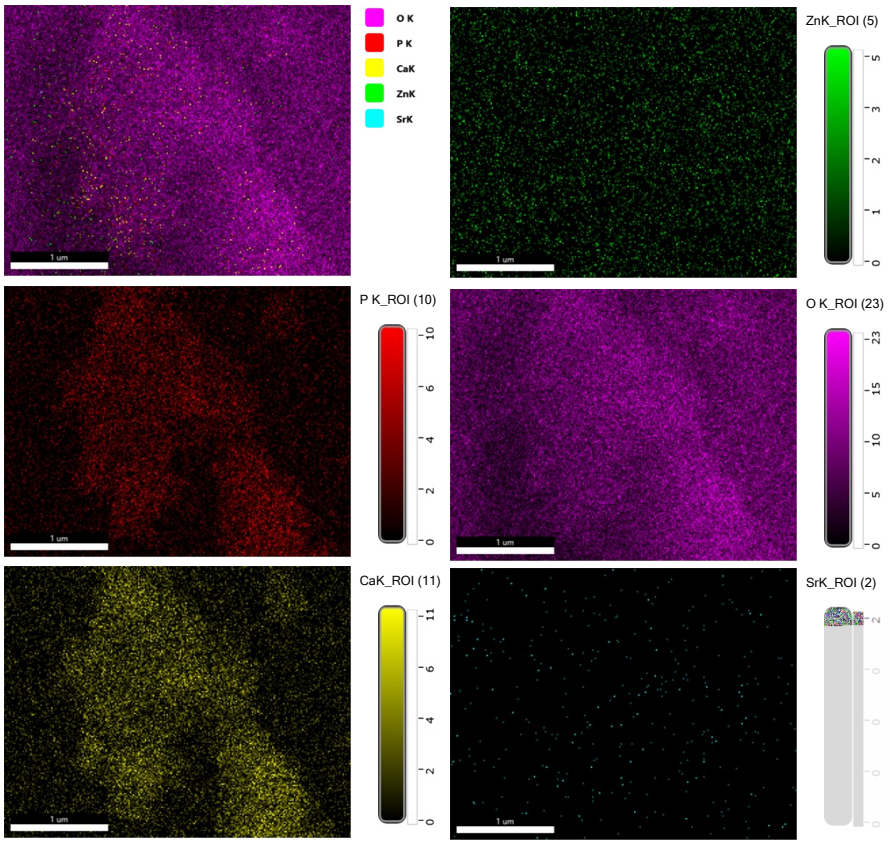

Figure S8. EDX mapping of ZnSr-HAp nanoparticles.

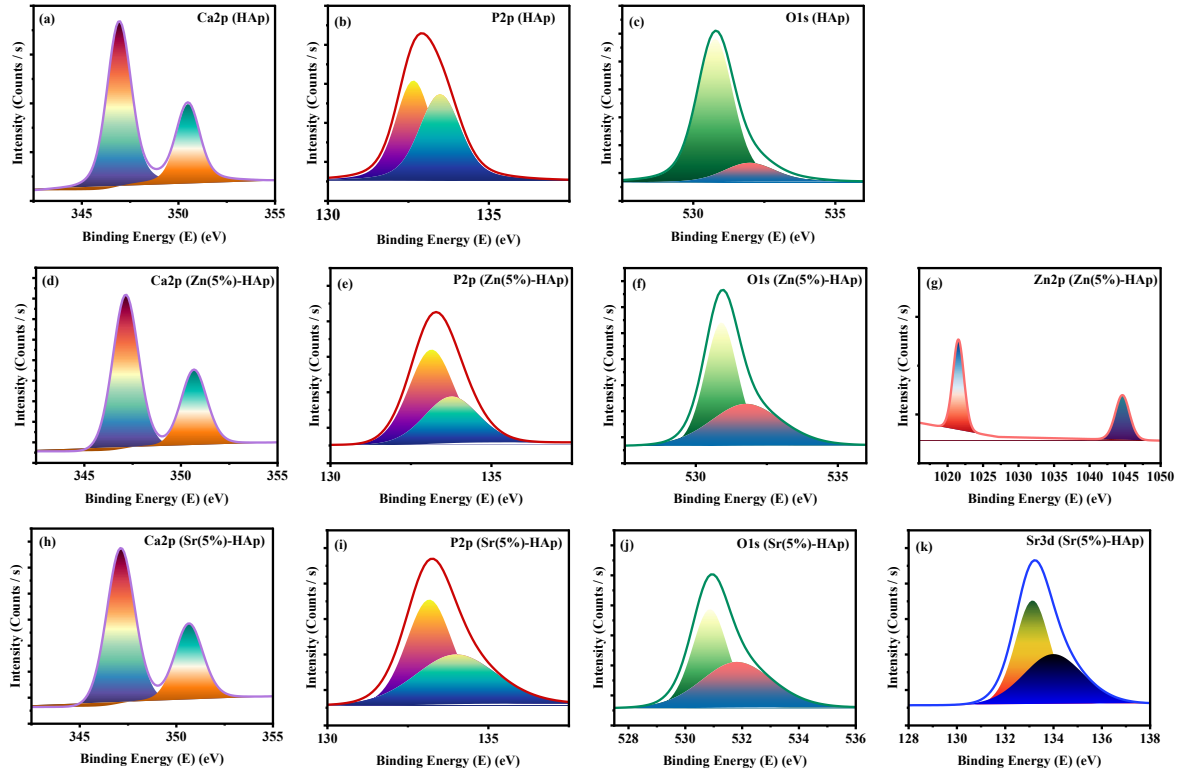

Figure S9. High-resolution spectra of (a-c) pristine HAp, (d-g) Zn(5%)-HAp, and (h-k) Sr(5%)-HAp, confirming elemental composition and oxidation states.

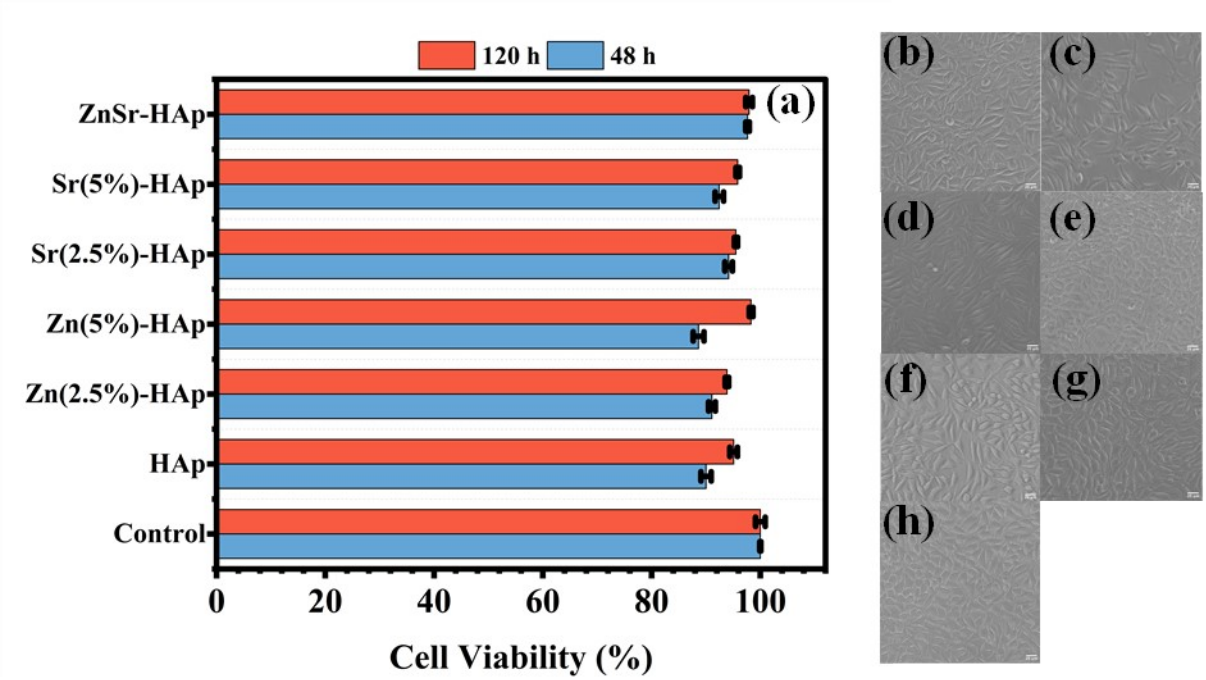

Figure S10. Cytocompatibility assessment of ion-substituted hydroxyapatite nanoparticles. (a) Quantitative cell viability analysis (MTT assay) after 48 h & 120 h culture with L929 fibroblasts. Representative light microscopy images of cells cultured after 120 h with: (b) control, (c) pristine HAp, (d) 2.5% Zn-HAp, (e) 5% Zn-HAp, (f) 2.5% Sr-HAp, (g) 5% Sr-HAp, and (h) ZnSr-HAp. Scale bars: 20 μm.

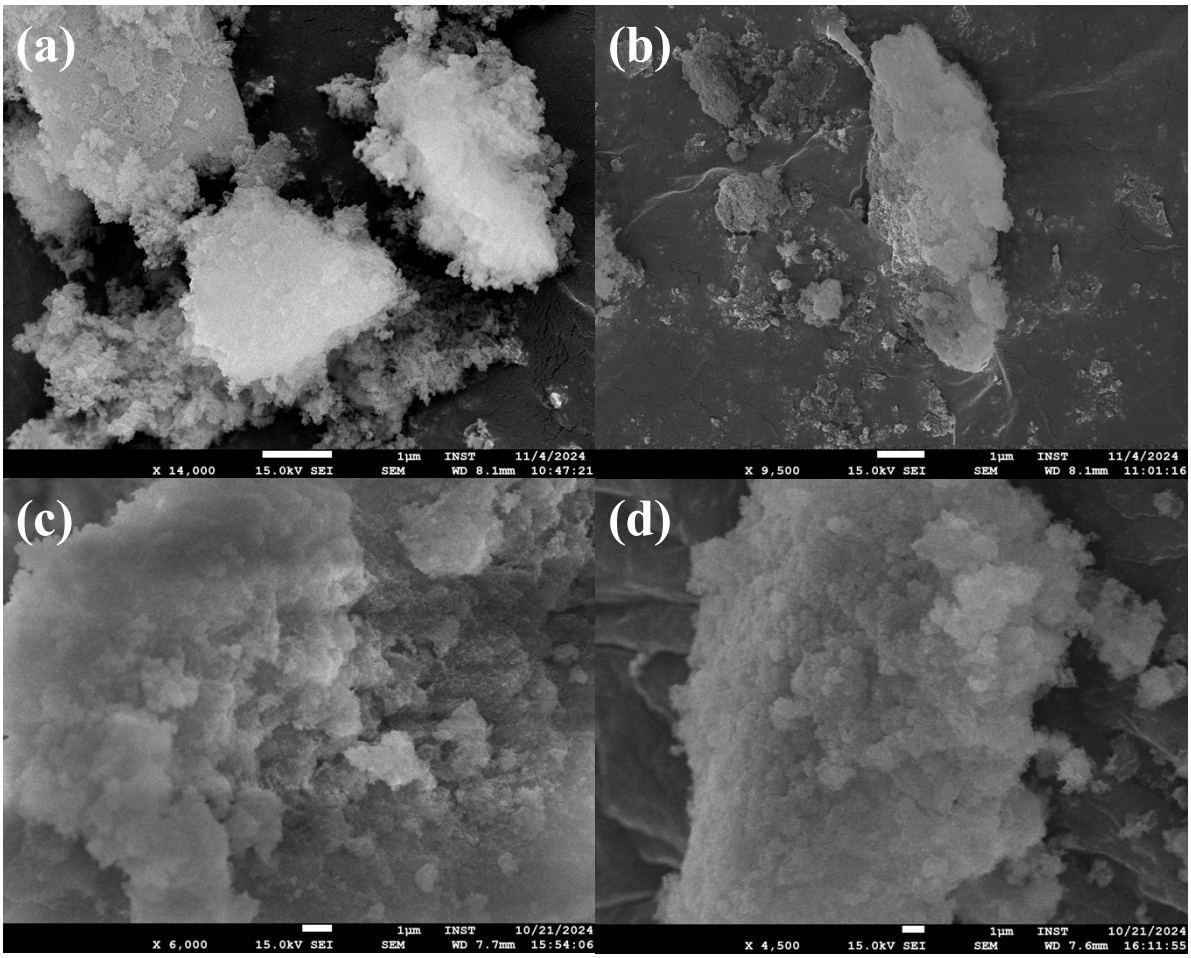

Figure S11. SEM images showing mineralization behavior after 14 days in simulated body fluid (SBF): (a) pristine HAp, (b) 5% Zn-HAp, (c) 5% Sr-HAp, and (d) ZnSr-HAp nanoparticles. Scale bars: 1 µm.

2.4 Hemocompatibility Assay of Zn-Sr-HAp nanoparticles

The hemocompatibility of the prepared nanoparticles was assessed using the *hemolysis* assay (ASTM F756–0). Initially, goat blood of 5 mL was obtained from local butcher shop and then subjected to three rounds of centrifugation for 10 min at 4000 rpm after adding 1.5 mg of ethylenediaminetetraacetic acid (EDTA). Subsequently, the resulting material was washed with phosphate buffered saline (PBS). Red blood cells (RBC) were collected through removing the supernatant/white blood cells. The recovered red blood cells were gently mixed with an equal amount of PBS. PBS and water were used as negative and positive controls, respectively, in a certain blood-to-solution ratio. Subsequently, a certain concentration was extracted into the Eppendorf tubes and combined with 950 µl of PBS and 50 µl of the previously made RBC. Then the prepared samples were incubated at 37 °C for a duration of 45 minutes. Subsequently, the mixture was subjected to centrifugation at a speed of 10000 revolutions per minute for a

duration of 5 minutes. The UV-vis spectrometer was used to measure the absorbance of the supernatant layer at a wavelength of 540 nm to evaluate the hemocompatibility of the samples.

The hemocompatibility of prisitn, Zn (5%), Sr (5%), and ZnSr substituted HAp nanoparticles was examined and the results are shown in Figure S11(a). The haemolytic activity of pristine, Zn, Sr, and ZnSr substituted HAp nanoparticles shows less 1% of lysis for two different concentrations of the nanoparticles. The 2.5 mg of samples treated with blood shows significantly less haemolysis rate compared to 5 mg. Additionally, 5 mg of Zn (5%), and ZnSr substituted HAp nanoparticles treated blood samples shows 0.78 and 0.83% of haemolysis, respectively compared to the positive control. As per ASTM F 756-08 [37], a hemolysis rate less than 5% is considered safe, while haemolysis rate higher than five percentage indicate a potential risk. The prepared samples demonstrated hemocompatibility, indicating they are safe for tissue engineering applications especially for bone regeneration application.

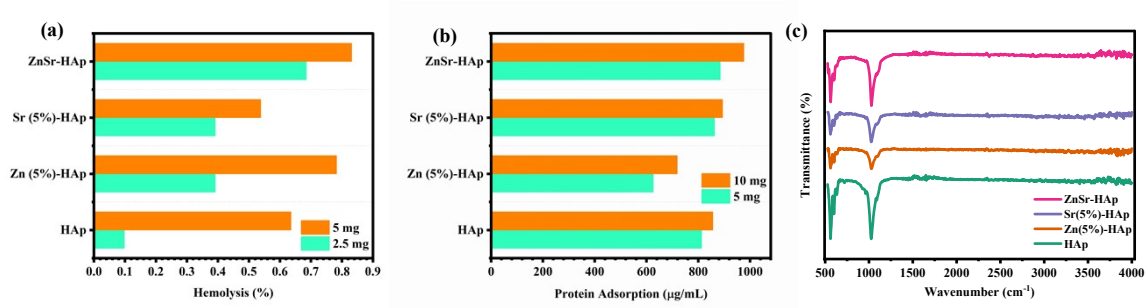

Figure S12. Biocompatibility and protein interaction studies. (a) Hemolysis assay of pristine HAp, Zn (5%)-HAp, Sr (5%)-HAp, and ZnSr-HAp nanoparticles. (b) Quantitative analysis of protein adsorption on nanoparticle surfaces. (c) FTIR spectra showing protein-nanoparticle interactions after adsorption, with amide I (1600-1700 cm^{-1}) and amide II (1480-1580 cm^{-1}) bands indicated.

Firstly, 1 mg of prepared samples were immersed in a test tube containing 1 ml of BSA and 2 ml of double-distilled water. After 3 h of incubation, Folin-Ciocalteu (F-C) reagent was added to 4.5 ml of supernatant to determine peptide bond for 30 min at 37 °C. Colour change from blue to green was observed after 30 minutes of incubation. At 660 nm, the absorption was measured using UV-vis spectrometer to determine the protein adsorption by the samples. Protein adsorption is essential for the bone repair and regeneration because it plays an important initial and critical role in the interaction between the biomaterials and the biological environment. The amount protein adsorption by pristine HAp, Zn (5%)-HAp, Sr (5%)-HAp, and ZnSr-HAp nanoparticles was estimated and presented in Figure 7(b). The protein

adsorption of the samples revealed increase of protein uptake with the increase of sample amount. The 5% Zn substituted hydroxyapatite reveals less amount of protein adsorption among other samples. The Sr (5%)-HAp exhibit higher protein adsorption than the pristine hydroxyapatite and Zn-HAp. The enhanced protein adsorption due to the reduction in the particle size. The Zn and Sr substituted HAp nanoparticles demonstrate higher protein adsorption for both 5 mg and 10 mg. The 5% Zn incorporated HAp shows lower protein adsorption due to the elongated morphology, while other samples show higher protein adsorption owing to rod-like morphology. The greater adsorption capacity is attributed to its larger surface area of the needle-shaped ZnSr-HAp morphology and semicrystalline nature. The protein adsorption of the samples was further confirmed by the FTIR analysis (Figure S11(c)). FTIR spectra exhibits the presence of hydroxyl and phosphate functional groups of the prepared samples. The additional bending vibrational and stretching vibrational band present in the samples confirms the successful loading of BSA protein. The presence of both prepared nanoparticles OH groups and the adsorbed BSA contribute to the broad adsorption peaks seen for the OH stretching vibration. Additionally, the electrostatic attraction between prepared nanoparticles and protein is crucial for surface adsorption. The adsorption of protein on prepared nanoparticles is due to the electrostatic interaction between the cations and anions present in both the nanoparticles and the protein [39,40]. The high adsorption capacity of prepared nanoparticles makes them a viable material for bone tissue engineering and as a potential medium for delivering proteins in the future.

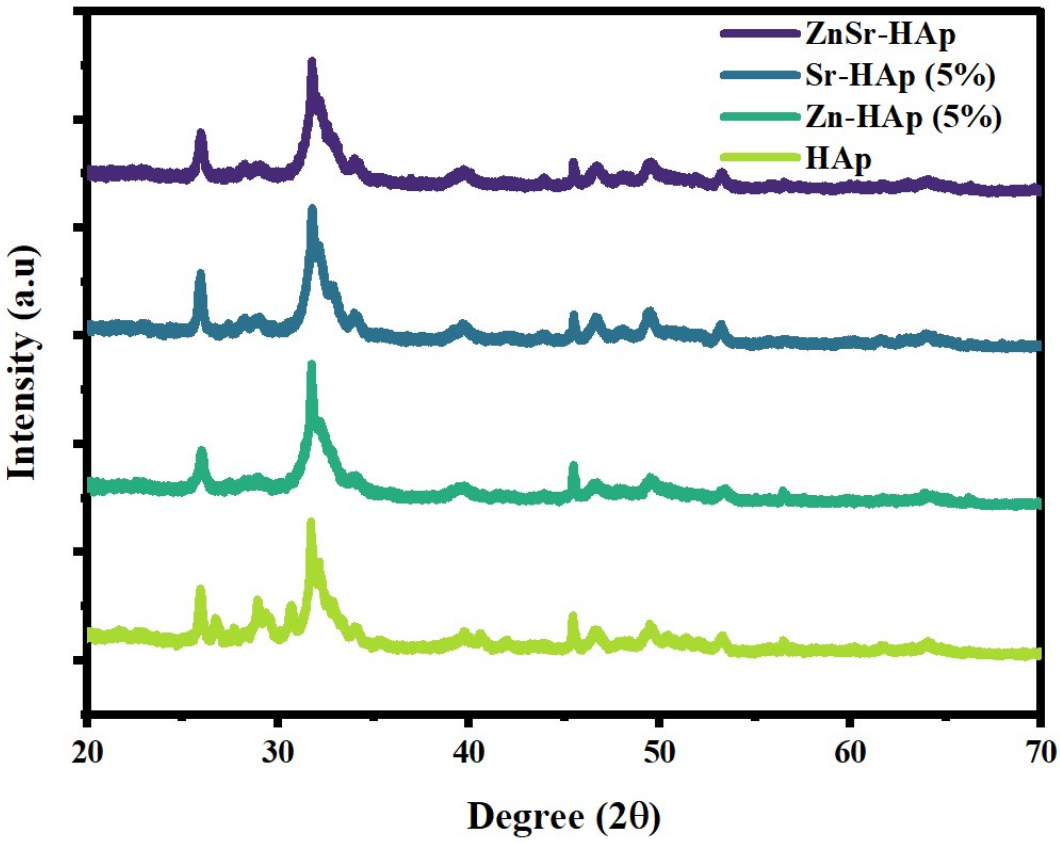

Figure S13. XRD pattern of the samples collected after 60 days of ion release in SBF solution